Acta Pharmaceutica Sinica B 2024;14(10):4577–4590

Chinese Pharmaceutical Association
Institute of Materia Medica, Chinese Academy of Medical Sciences

Acta Pharmaceutica Sinica B

www.elsevier.com/locate/apsb
www.sciencedirect.com

ORIGINAL ARTICLE

Simultaneous enhancement of cellular and humoral immunity by the lymph node-targeted cholesterolized TLR7 agonist liposomes

Dandan Wan[a], Ziyi Bai[a], Yu Zhang[a], Li Chen[a], Haiying Que[a], Tianxia Lan[a], Weiqi Hong[a], Jiayu Huang[a], Cai He[a], Yuquan Wei[a], Qiang Pu[b,*], Xiawei Wei[a,*]

[a]*Laboratory of Aging Research and Cancer Drug Target, State Key Laboratory of Biotherapy and Cancer Center, National Clinical Research Center for Geriatrics, West China Hospital, Sichuan University, Chengdu 610041, China*
[b]*Department of Thoracic Surgery, National Frontier Center of Disease Molecular Network, West China Hospital, Sichuan University, Chengdu 610041, China*

Received 23 February 2024; received in revised form 14 May 2024; accepted 16 May 2024

KEY WORDS

TLR7 agonist;
Cationic liposomes;
Lymph node;
Cancer nanovaccines;
Immunotherapy;
Cross-presentation;
Cellular immunity;
Humoral immunity

Abstract Toll-like receptor (TLR) agonists, as promising adjuvants and immunotherapeutic agents, have the potential to enhance immune responses and modulate antigen-dependent T-cell immune memory through activation of distinct signaling pathways. However, their clinical application is hindered by uncontrolled systemic inflammatory reactions. Therefore, it is imperative to create a vaccine adjuvant for TLR receptors that ensures both safety and efficacy. In this study, we designed lymph node-targeted cholesterolized TLR7 agonist cationic liposomes (1V209-Cho-Lip$^+$) to mitigate undesired side effects. Co-delivery of the model antigen OVA and cholesterolized TLR7 agonist facilitated DC maturation through TLR activation while ensuring optimal presentation of the antigen to CD8$^+$ T cells. The main aim of the present study is to evaluate the adjuvant effectiveness of 1V209-Cho-Lip$^+$ in tumor vaccines. Following immunization with 1V209-Cho-Lip$^+$+OVA, we observed a pronounced "depot effect" and enhanced trafficking to secondary lymphoid organs. Prophylactic vaccination with 1V209-Cho-Lip$^+$+OVA significantly delays tumor development, prolongs mouse survival, and establishes durable immunity against tumor recurrence. Additionally, 1V209-Cho-Lip$^+$+OVA, while used therapeutic tumor vaccine, has demonstrated its efficacy in inhibiting tumor progression, and when combined with anti-PD-1, it further enhances antitumor effects. Therefore, the co-delivery of antigen and lymph node-targeted cholesterolized TLR7 agonist shows great promise as a cancer vaccine.

*Corresponding authors.
E-mail addresses: puqiang100@163.com (Qiang Pu), xiaweiwei@scu.edu.cn (Xiawei Wei).
Peer review under the responsibility of Chinese Pharmaceutical Association and Institute of Materia Medica, Chinese Academy of Medical Sciences.

https://doi.org/10.1016/j.apsb.2024.06.006

1. Introduction

Immunotherapy through vaccination is a valuable and cost-effective approach for preventing infectious diseases and cancer. Among various tumor immunotherapies, cancer vaccines have garnered extensive attention due to their specific immunity, long-term immunological memory, and potential for tumor prevention[1-4]. Although the protein or peptide subunit vaccines have received rapid development for their ease of manufacturing, improved safety, and enhanced quality control, their rapid clearance and poor immunogenicity resulted in weak and short-lived anti-tumor immune responses[5]. To achieve robust and durable adaptive anti-tumor immune responses in cancer vaccines, a proper adjuvant accomplishing antigen delivery as well as immunological enhancement is important[6,7]. The most commonly used aluminum-based adjuvant lacks the ability to perform desired antitumor immune responses due to its limited capacity in stimulating cell-mediated immunity[8]. Hence, it is particularly urgent to explore potent, effective and safe adjuvants that can significantly enhance humoral and cellular immune responses in clinical vaccination.

Dendritic cells (DCs) represent the most powerful and pivotal antigen presenting cells (APCs) responsible for efficient uptake and presentation of antigens, initiation of immune responses, and regulation of humoral and cellular immunity[9-11]. By activating APCs, adjuvants obtain the probability to release the natural killing function of cytotoxic T lymphocytes (CTLs) to eliminate cancer or pathogens. Various adjuvants, such as TLR agonists, activate innate immune receptors on APCs, resulting in the presentation of antigens by APCs, release of cytokines, and subsequent provision of costimulatory signals to CD8 T cells[12,13]. An ideal cancer vaccine should not only create a "depot effect" at the site of injection to sustain antigen exposure to DCs, but also deliver vaccine to the draining lymph nodes (LNs) to activate T and B cells which is essential to induce valid and long-term antitumor immunity[14,15]. To achieve these, a promising approach entails the utilization of a vaccine based on nanoparticles that can safeguard antigens against degradation, activate DCs, and co-deliver antigens and adjuvant to draining LNs, initiating the immune system[7,16,17].

TLRs have long been considered as adjuvants in adaptive immune responses[18,19]. As the key sensors of the innate immunity, TLRs *via* the adapter proteins (MyD88, TRAM, TRIF, and MAL) pathway to activate a diverse range of immune cells, especially the DCs[20-22]. Meanwhile, the utilization of TLR agonists as immunoadjuvants through a nanoparticle delivery system can significantly augment immune responses and significantly improve antigen cross-presentation[6,23-26]. However, they have been reported to be quite toxic in some instances, possibly due to their widespread distribution within the body and subsequent activation of myeloid cells, leading to a cytokine storm[27-29]. Although nanoparticle delivery systems can reduce the toxicity of TLR agonists to some extent, the complexity and low biocompatibility of many nanoparticle delivery systems also limit the clinical application of TLR agonists. Therefore, there is an urgent need for a nano-drug delivery system that can reduce the toxicity of TLR agonists and enable clinical transformation. In our previous study, we found that encapsulation of the cholesterolized TLR7 agonist within neutral liposomes not only exerted minimal toxic effects but also enhanced its immunostimulatory and immunotherapeutic breadth[30]. The present work, aimed to encapsulate the cholesterolized TLR7 agonist in cationic liposomes (1V209-Cho-Lip$^+$) and evaluate its vaccine potency for long-term tumor prevention. Cationic liposomes have been reported to exhibit higher immunogenicity compared to neutral or anionic liposomes[31,32]. Among various nano-systems, 1V290-Cho-Lip$^+$+OVA holds promise as a potential tumor vaccine platform for future translational studies in tumor immunotherapy due to its facile synthesis, availability of raw materials, and improved safety[33,34]. Our results indicated that immunization with 1V209-Cho-Lip$^+$ adjuvanted ovalbumin (OVA) stimulated antigen-specific humoral and CTL responses, leading to the suppression of tumor progression and extended survival duration in mice. Additionally, we observed that the cationic liposomal vaccine 1V209-Cho-Lip$^+$+OVA induced a durable CD8$^+$ memory T-cell immunity specific to the antigen, effectively preventing tumor formation even six months after initial immunization. Meanwhile, the cationic liposomal vaccine 1V209-Cho-Lip$^+$+OVA effectively suppressed tumor progression in the therapeutic B16F10-OVA melanoma and E.G7-OVA lymphoma models when combined with immune checkpoint blockade (ICB). Scheme 1 demonstrates the targeted effective delivery of both antigen and TLR7 agonist by 1V209-Cho-Lip$^+$+OVA cationic liposomes for cancer immunotherapy.

2. Materials and methods

2.1. Materials

The compound 1V209 was acquired from Selleck (Houston, USA). DOTAP (chloride salt) and DSPE-PEG$_{2000}$ (ammonium salt) were obtained from Avanti Polar Lipids (Alabaster, USA). Albumin from chicken egg white (OVA) and cholesterol were sourced from Sigma−Aldrich (St. Louis, USA). The B16F10-OVA and E.G7-OVA mouse melanoma cell lines were sourced from the Chinese Academy of Sciences Cells Bank (Shanghai, China). Female C57BL/6J mice were procured from Huafukang Biotechnology Co., Ltd. (Beijing, China). All animal experiments conducted adhered to the guidelines evaluated and approved by the Ethics Committee of Sichuan University (20210409044).

2.2. Preparation and characterization of cationic liposomes (1V209-Cho-Lip$^+$+OVA and Blank-Lip$^+$+OVA)

Firstly, DOTAP (chloride salt), cholesterol, 1V209-Cho, DSPE-PEG$_{2000}$ (ammonium salt) (molar ratio = 62:32:3:3) were dissolved in chloroform/methanol (v/v = 10:1). The solvent was then evaporated using rotary evaporation at 37 °C to form a lipid film. Subsequently, the lipid film was hydrated in PBS for 1 h at 37 °C followed by intermittent sonication in water for 30 min and probe sonication at an intensity of 80 W for 120 s to form cationic 1V209-cholesterolated liposomes (1V209-Cho-Lip$^+$), and then the OVA was added which can bound with DOTAP through

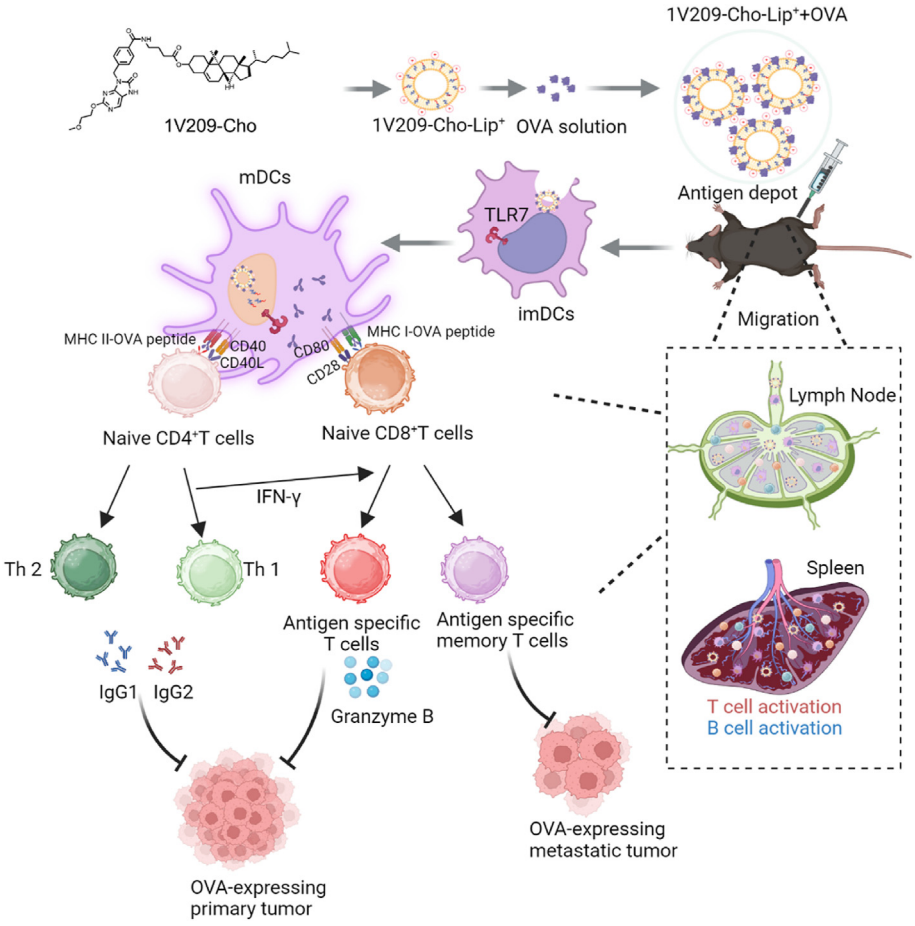

Scheme 1 1V209-Cho-Lip^{+}+OVA effectively co-delivers antigen and TLR7 agonist, thereby augmenting both humoral and cellular immunity to exert a superior anti-tumor effect.

electrostatic adherence by vibrating at 37 °C for 1 h, the 1V209-Cho-Lip^{+}+OVA were obtained. Blank-Lip^{+}+OVA were prepared by a similar method, only without 1V209-Cho. The DLS technique (Malvern Zetasizer Nano ZS) was employed for size distribution and zeta potential analysis, while TEM imaging (H-600, Hitachi, Japan) was utilized to capture the morphologies.

2.3. *The uptake of cationic liposomes by DCs in vitro*

Murine DCs were seeded into 24-well titer plates. Then OVA^{F}, Blank-Lip^{+}+OVA^{F} and 1V209-Cho-Lip^{+}+OVA^{F} (equivalent OVA-FITC) were added and further incubated with DCs for 4 h. After incubation, the liquid in the container was aspirated and the cells were rinsed with PBS and then suspended in PBS followed by flow cytometry analysis. DCs incubated with PBS were used as a control.

2.4. *BMDCs activation assays in vitro*

Bone marrow-derived dendritic cells (BMDCs) were obtained from C57BL/6J mice and then cultured for a period of 6 days to obtain immature BMDCs. Then the immature BMDCs were added to a 24-well cell culture plate (10^{6} per well) and incubated overnight. Then, PBS, OVA, Blank-Lip^{+}+OVA and 1V209-Cho-Lip^{+}+OVA were added and incubated with DCs for 48 h. After incubation, DCs were stained with anti-mouse CD11c percp-Cy5.5, anti-mouse CD86 FITC, anti-mouse CD80 PE and anti-mouse CD40 APC for 30 min in ice for flow cytometry detection.

2.5. *Measurement of cross-priming of CD8 T cells in vitro*

In the cross-presentation of antigens studies, the Mouse CD8^{+} T Cell Isolation Kit was used to isolate CD8 T cells from OT-1 transgenic mice and subsequently labeled with CFSE. Subsequently, 3×10^{5} CFSE-labeled CD8^{+} T cells and the activated DCs were co-cultured in RPMI 1640 medium for 72 h. After, the cells were gathered and subjected to staining with anti-mouse CD3 Percp-Cy5.5, anti-mouse CD8 PE, and anti-mouse CD69 BV421 (BioLegend). Finally, the cells underwent two washes using PBS and were examined using flow cytometer.

2.6. *Lymphatic tracking of labeled cationic liposomes in vivo*

To visualize the real-time behavior of different cationic liposomes after administration, OVA-FITC was encapsulated into different cationic liposomes instead of OVA and intramuscularly injected into C57BL/6J mice at a dose of 50 μg OVA-FITC on their left leg. Lymphatic tracking of labelled cationic liposomes was real-time monitored at the draining inguinal lymph nodes. The Lumina III Imaging System (PerkinElmer, USA) was utilized for *in vivo* fluorescent imaging at 4, 12, and 24 h. At last time point, the mice

were autopsied, and inguinal lymph nodes and popliteal lymph nodes were excised and fixed for subsequent imaging.

2.7. Immunoprophylaxis experiments

In this experiment, female C57BL/6J mice were randomly assigned to four groups PBS, OVA, Blank-Lip$^+$+OVA and 1V209-Cho-Lip$^+$+OVA ($n = 8$), and intramuscularly immune (25 μg/rat OVA and 5 μg/rat 1V209-Cho) on Days 0, 14 and 21. Subsequently, on Day 28, the right flank of the mice was subcutaneously inoculated with either B16F10-OVA or E.G7-OVA cells (1×10^6 cells). Tumor growth and survival rate were calculated.

2.8. Mechanism of immunoprophylaxis

To investigate the mechanism of immunoprophylaxis, mice were sacrificed seven days after their final immunization ($n = 5$). Serum of mice was obtained to analysis of OVA specific IgG and IgG subtypes using ELISA analysis. The amounts of INF-γ, Granzyme-B, TNF-α, IL-6 and IL-10 in the serum or culture supernate were quantified using ELISA kits. Spleens and inguinal lymph nodes were collected, triturated and filtered through a 70 μm filter, then the dissociated cells were stained with anti-mouse antibody (BioLegend). The stained cells were tested using a NovoCyte Flow Cytometer (ACEA Biosciences, Inc.). In addition, splenocytes were restimulated with $OVA_{257\text{-}264}$ (10 μg/mL) for 3 days and stained with anti-mouse CD3 Percp-Cy5.5, anti-mouse CD8 BV510, anti-mouse SIINFEKL-MHCI PE, anti-mouse IFN-γ PE-Cy7 and anti-mouse Granzyme-B AF647 (BioLegend). To assess the cytotoxic potential of T cells, Splenic lymphocytes were subsequently re-stimulated with CD8$^+$-specific $OVA_{257-264}$ peptides (10 μg/mL) for a duration of 3 days. Then the lymphocytes (effector cells) and CFSE labeled B16F10-OVA cells (target cells) or B16F10 cells (negative control target cells) were incubated in different E:T ratios for 6 h. The frequencies of B16F10-OVA (CFSE high) cells were tested and calculated the percent specific killing.

2.9. 1V209-Cho-Lip$^+$+OVA induced persistent humoral and cellular immune response and prevented tumor formation

Female C57BL/6J mice were divided into PBS, OVA, Blank-Lip$^+$+OVA and 1V209-Cho-Lip$^+$+OVA groups ($n = 5$), and intramuscularly immunized (25 μg/rat OVA and 5 μg/rat 1V209-Cho) on Days 0, 14 and 21. Blood samples were collected from eye sockets of mice at the 5th and 6th months following the initial injection. IgG subtypes in the collected sera were analyzed using ELISA with appropriate sample titrations. At six months after the first injection, animals received a subcutaneous inoculation of 1×10^6 B16F10-OVA cells. The size of the tumor was assessed every two days for a period of twenty days. Subsequently, animals were euthanized and blood as well as spleen samples were obtained, then the single cell suspensions were stained with anti-mouse CD3 Percp-Cy5.5, anti-mouse CD19 PE, anti-mouse IgD APC, anti-mouse CD27 FITC, anti-mouse IgM BV421 (BioLegend).

2.10. ELISPOT assays

Immulon 2 HB plates coated with anti-IFN-γ antibody were blocked with PBS-BSA for use in the assay. Splenic lymphocytes were seeded onto the plates supplemented with $OVA_{257\text{-}264}$ peptide or media alone. After incubated for 18 h, detection of IFN-γ-producing CD8$^+$ T-cell spots was achieved by using a biotinylated anti-IFN-γ antibody followed by alkaline phosphatase streptavidin and BCIP dissolved in low melting agarose solutions. Spot analysis was performed using the Mabtech IRIS FluoroSpot/ELISpot reader.

2.11. Immunotherapeutic experiment in vivo

Subcutaneous inoculation of either 3×10^5 B16F10-OVA or E.G7-OVA cells on mice. Mice with established tumors were randomly divided into six groups: PBS group, OVA group, Blank-Lip$^+$+OVA group, 1V209-Cho-Lip$^+$+OVA group, Anti-PD-1 group and 1V209-Cho-Lip$^+$+OVA + Anti-PD-1 group ($n = 8$). The 1V209-Cho-Lip$^+$+OVA vaccine was intramuscularly administered on Day 5, once every seven days, three times in total (25 ug/rat OVA and 5 ug/rat 1V209-Cho). And the Anti-PD-1 (100 ug/rat) was injected intraperitoneally, once every 3 days, six times in total. Tumor growth and mouse survival were monitored.

2.12. Pathological evaluation of vital organs

Female C57BL/6J mice were intramuscularly immunized with 1V209-Cho-Lip$^+$+OVA. After three times immunization, the heart, liver, spleen, lung, and kidney were obtained and then fixed in a buffered formalin solution (4%) for 72 h. Subsequently, the samples underwent embedding in paraffin and sectioning into approximately 3 μm thick slices. These sections underwent dewaxing using ethanol and xylene before being stained with hematoxylin-eosin (H&E).

2.13. Statistical analysis

The mean ± standard error of the mean (SEM) was used to present the data. Pairwise comparisons were assessed for statistical significance using two-tailed Student's *t*-tests, while multiple group comparisons were evaluated using one-way ANOVA. Significance levels of $P < 0.05$, $P < 0.01$, and $P < 0.001$ were considered to indicate significant differences (remarked with *, ** and ***, respectively).

3. Results and discussion

3.1. Preparation and characterization of 1V209-Cho-Lip$^+$+OVA vaccine

1V209-Cho was synthesized according to our earlier report[30]. The cationic lipid material DOTAP was used to prepare cationic liposome 1V209-Cho-Lip$^+$ by the thin film hydration method. Subsequently, the 1V209-Cho-Lip$^+$+OVA complex was formed by facilely mixing the 1V209-Cho-Lip+ with an OVA solution. Meanwhile, blank cation liposomes (Blank-Lip$^+$) without 1V209-Cho component were used as a control. DLS analysis indicated that the hydrodynamic diameter of 1V209-Cho-Lip$^+$+OVA was approximately 190 nm, larger than that of 1V209-Cho-Lip$^+$ (Fig. 1A and B). Meanwhile, the FE-TEM showed the mean sizes of 1V209-Cho-Lip$^+$+OVA were approximately 200 nm and larger than 1V209-Cho-Lip$^+$ which were consistent with DLS data (Fig. 1A and B). The mean sizes of Blank-Lip$^+$+OVA were also larger than that of Blank-Lip$^+$ (Supporting Information Figs. S1A and S1B). The combined results of DLS and FE-TEM confirmed

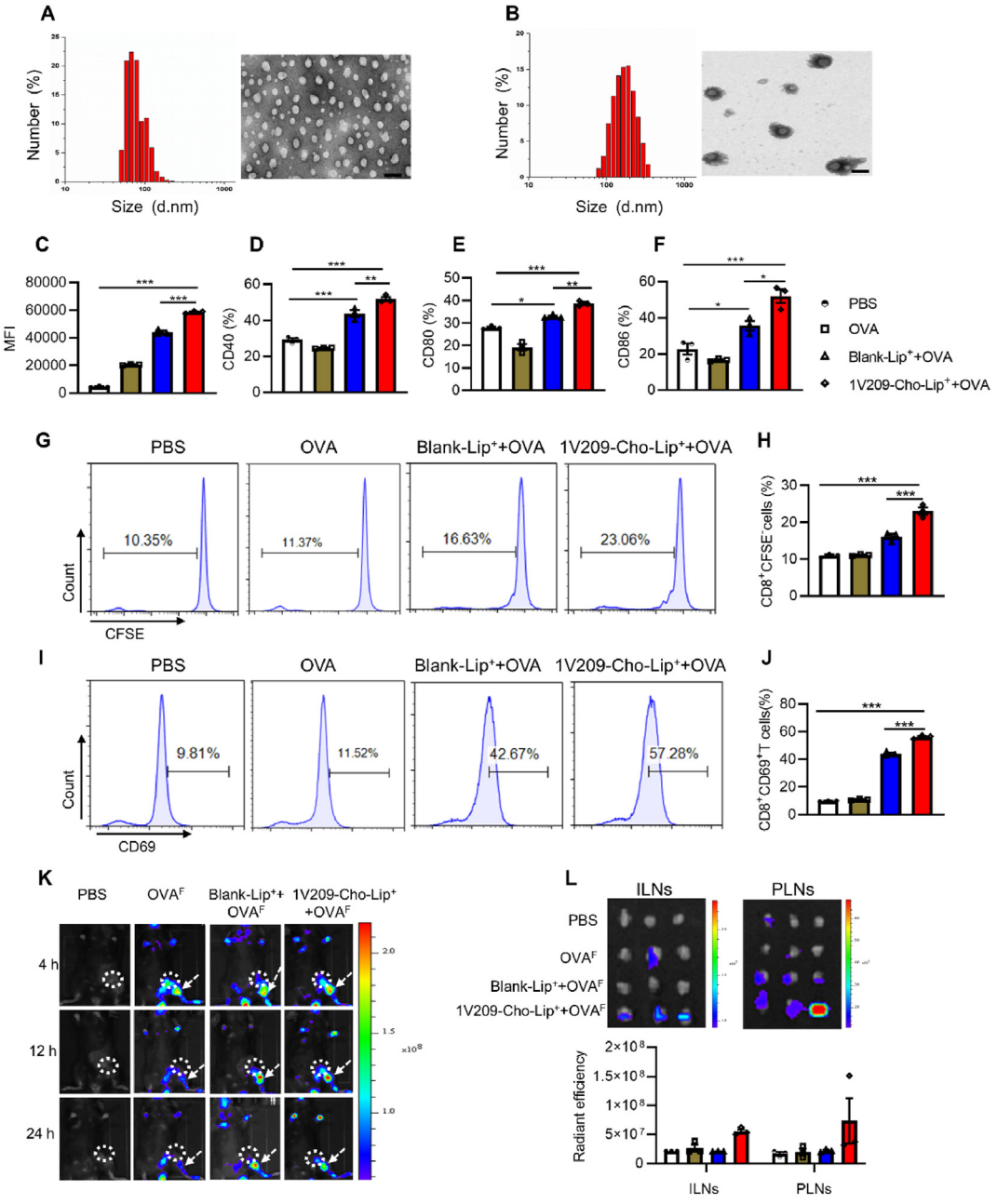

Figure 1 (A) DLS and TEM image of 1V209-Cho-Lip$^+$, scale bar = 200 nm. (B) DLS and TEM image of 1V209-Cho-Lip$^+$+OVA, scale bar = 200 nm. (C) The cellular uptake of BMDCs were measured by FACS analysis. (D−F) The expression levels of (D) CD40, (E) CD80, and (F) CD86 on DCs. (G and H) Representative flow cytometry pictures and quantification of CFSE-OT-I CD8 T cells after coculture with DC activated by PBS, OVA, Blank-Lip$^+$+OVA, and 1V209-Cho-Lip$^+$+OVA for 72 h. (I and J) Representative flow cytometry pictures and quantification of CD69 expression on OT-I CD8 T cells after coculture with DC activated by PBS, OVA, Blank-Lip$^+$+OVA, and 1V209-Cho-Lip$^+$+OVA for 72 h. (K) *In vivo* fluorescent imaging of mice. (L) *Ex vivo* imaging and semiquantification of in inguinal and popliteal lymph node fluorescence at 24 h post-injection. Data are presented as mean ± SEM ($n = 3$). *$P < 0.05$, **$P < 0.01$, ***$P < 0.001$.

the strong capacity of 1V209-Cho-Lip$^+$ and Blank-Lip$^+$ to capture OVA and generate1V209-Cho-Lip$^+$+OVA and Blank-Lip$^+$+OVA complexes. Both 1V209-Cho-Lip$^+$+OVA and Blank-Lip$^+$+OVA were of similar ζ potential (20 ± 0.24 mV), which were lower than those of Blank-Lip$^+$ and 1V209-Cho-Lip$^+$ (35 ± 1.02 mV). Additionally, the encapsulation efficiency of OVA was 90 ± 1.24%.

3.2. *1V209-Cho-Lip$^+$+OVA promotes DCs uptake, activation and the antigen cross-presentation*

Efficient internalization of 1V209-Cho-Lip$^+$+OVA by DCs is crucial, as DCs are potent APCs to activate native T cells. To investigate the cellular uptake of 1V209-Cho-Lip$^+$+OVA, fluorescein isothiocyanate (FITC)-labelled OVA was used to construct

fluorescent 1V209-Cho-Lip$^+$+OVA^F. PBS, OVA^F, and Blank-Lip$^+$+OVA^F were included for comparison purposes. Flow cytometry analysis revealed that both 1V209-Cho-Lip$^+$+OVA^F and Blank-Lip$^+$+OVA^F groups exhibited efficient endocytosis by DCs compared to free OVA^F (Fig. 1C and Fig. S1C). In contrast, a significantly higher fluorescence of 1V209-Cho-Lip$^+$+OVA^F group than Blank-Lip$^+$+OVA^F was attributed to the component of the 1V209-Cho, which supported our earlier report[30]. These results demonstrate the superior uptake capability of 1V209-Cho-Lip$^+$+OVA^F by DCs.

Having confirmed the favorable cellular uptake of DCs to 1V209-Cho-Lip$^+$+OVA, we proceeded to investigate its potential in enhancing DC maturation and subsequent immune responses. As depicted in Fig. 1D−F, compared to the PBS group, incubation with 1V209-Cho-Lip$^+$+OVA resulted in a significant expression of CD40 (1.77-fold), CD80 (1.38-fold) and CD86 (2.20-fold), the important indicators of DC maturation. In contrast, incubation with Blank-Lip$^+$+OVA only observed a slight upregulation of costimulatory molecules, owing to the intrinsic immunostimulatory properties of cationic liposome[35,36]. These findings show that 1V209-Cho-Lip$^+$+OVA is a potent nanovaccine capable of promoting DC maturation.

Efficient cross-presentation of extracellular proteins by DCs is crucial for initiating immune responses[37]. Subsequently, we investigated whether 1V209-Cho-Lip$^+$+OVA could enhance antigen cross-presentation by DCs. In this study, we utilized CD8$^+$ T cells from OT-1 mice to assess the ability of 1V209-Cho-Lip$^+$+OVA-stimulated DCs in conducting cross-presentation of soluble OVA. Flow cytometry analysis of CFSE fluorescence revealed a 2.1-fold increase in the proliferation of CD8$^+$ T cells upon co-culture with 1V209-Cho-Lip$^+$+OVA-treated DCs (Fig. 1G and H). Meanwhile, the CD8$^+$ T-cell activation upon co-culture with 1V209-Cho-Lip$^+$+OVA-treated DCs was 5.8-fold higher than PBS-treated DCs (Fig. 1I and J). In contrast, Blank-Lip$^+$+OVA-treated DCs had less effect on CD8$^+$ T-cell proliferation (Fig. 1G and H) and activation (Fig. 1I and J). Collectively, these findings demonstrate that *in vitro* treatment with 1V209-Cho-Lip$^+$+OVA can substantially enhance the ability of DCs to present extracellular antigens through cross-presentation, which may play a critical role in the initiation of antigen-specific CTL activity.

3.3. *In vivo biodistribution of the 1V209-Cho-Lip$^+$+OVA*

An effective vaccine delivery system necessitates the establishment of a "depot" at the injection site as well as efficient antigen transportation to the lymph nodes. In our previous study, we found that 1V209-Cho-Lip exhibited targeting and accumulation in lymph nodes[30]. Here, we evaluated the extent to which 1V209-Cho-Lip$^+$+OVA specifically targets the injection site and its associated draining lymph node, a feature closely linked to adjuvant potency. Mice were injected i.m. in the left leg with PBS, OVA^F, Blank-Lip$^+$+OVA^F and 1V209-Cho-Lip$^+$+OVA^F (equivalent dose of OVA^F) followed by full-body luminescence imaging of the fluorescence signal at 4, 12, and 24 h post-injection. As depicted in Fig. 1K and L, the fluorescence intensity in inguinal LNs (marked by white circle) of 1V209-Cho-Lip$^+$+OVA^F group was stronger than OVA^F and Blank-Lip$^+$+OVA^F group. Furthermore, this intensity remained consistently high even after 24 h following injection, suggesting a robust migration and retention of 1V209-Cho-Lip$^+$+OVA^F in inguinal LNs. Moreover, stronger fluorescence intensity was observed in the injection site (marked by white arrows) of 1V209-Cho-Lip$^+$+OVA^F and Blank-Lip$^+$+OVA^F group than OVA^F group at 12 and 24 h, which is consistent with previous reports, cationic liposomes have the capability to form a depot at the site of injection[38,39]. However, the fluorescence intensity in inguinal LNs (marked by white circle) of Blank-Lip$^+$+OVA^F group was weak. *Ex vivo* imaging revealed that the 1V209-Cho-Lip$^+$+OVA^F exhibited a stronger fluorescence intensity in inguinal and popliteal LNs compared to the Blank-Lip$^+$+OVA^F and OVA^F groups. Semi-quantification analysis of *ex vivo* imaging (Fig. 1L) demonstrated that the fluorescence intensity in inguinal and popliteal LNs of the group 1V209-Cho-Lip$^+$+OVA^F was 2.06-fold and 5.52-fold higher than that observed in the OVA^F group, respectively. Overall, 1V209-Cho-Lip$^+$+OVA^F exhibits both "depot effects" at the injection site and facilitates antigen delivery to draining LNs.

3.4. *Antitumor efficiency of 1V209-Cho-Lip$^+$+OVA as a prophylactic vaccine*

Inspired by the aforementioned findings, we subsequently assessed the *in vivo* immune-prophylactic efficacy of 1V209-Cho-Lip$^+$+OVA in B16F10-OVA melanoma model. Various vaccine groups were intramuscularly injected on Days 0, 14, 21 (Fig. 2A). Tumor cells were inoculated seven days following the completion of immunization. On Day 28, serum samples were collected to measure titers of OVA-specific IgG subclasses (IgG1 and IgG2a/b) using ELISA (Supporting Information Fig. S2A−S2D). Intramuscular immunization with Blank-Lip$^+$+OVA and 1V209-Cho-Lip$^+$+OVA all induced higher serum OVA-specific IgG levels compared with those induced by immunization with OVA and PBS (Fig. S2A), and the 1V209-Cho-Lip$^+$+OVA group induced the highest serum OVA-specific IgG levels. While immunization with Blank-Lip$^+$+OVA primarily induced Th2-related IgG1, 1V209-Cho-Lip$^+$+OVA elicited a balanced immune response by inducing both IgG1 and the Th1-related IgG2a and IgG2b (Fig. S2B−S2D). The 1V209-Cho-Lip$^+$+OVA group exerted potent tumor growth inhibition and maximum survival time compared to that from the Blank-Lip$^+$+OVA group, OVA group and the PBS group (Fig. 2B−F) and led to complete regression of the tumors in 62.5% of the mice (Fig. 2E and G). The Blank-Lip$^+$+OVA group exhibited a modest inhibition effect on tumor growth, attributed to the adjuvant properties of cationic liposomes. Overall, these findings demonstrate that 1V209-Cho-Lip$^+$+OVA could serve as an efficacious vaccine for preventing tumor development following OVA-expressing tumor cell inoculation.

3.5. *1V209-Cho-Lip$^+$+OVA elicited robust cellular immune responses in mice*

Next, we further investigate the immune prevention mechanism, as shown in Fig. 2H and J, the proportion of activated CD4$^+$ and CD8$^+$ T cells in draining inguinal lymph nodes significantly increased after immunization with 1V209-Cho-Lip$^+$+OVA (Supporting Information Fig. S3A and S3B), which are crucial for inducing a robust immune response and achieving effective immune prevention and protection. Vaccination is an effective strategy for preventing disease upon reinfection with pathogens. In general, upon reinfection, memory T cells that were generated during the initial infection can promptly initiate a cascade of immune responses. In our study, we evaluated memory T cells (both CD4$^+$ and CD8$^+$) from inguinal lymph nodes of mice that were immunized three times using FACS analysis

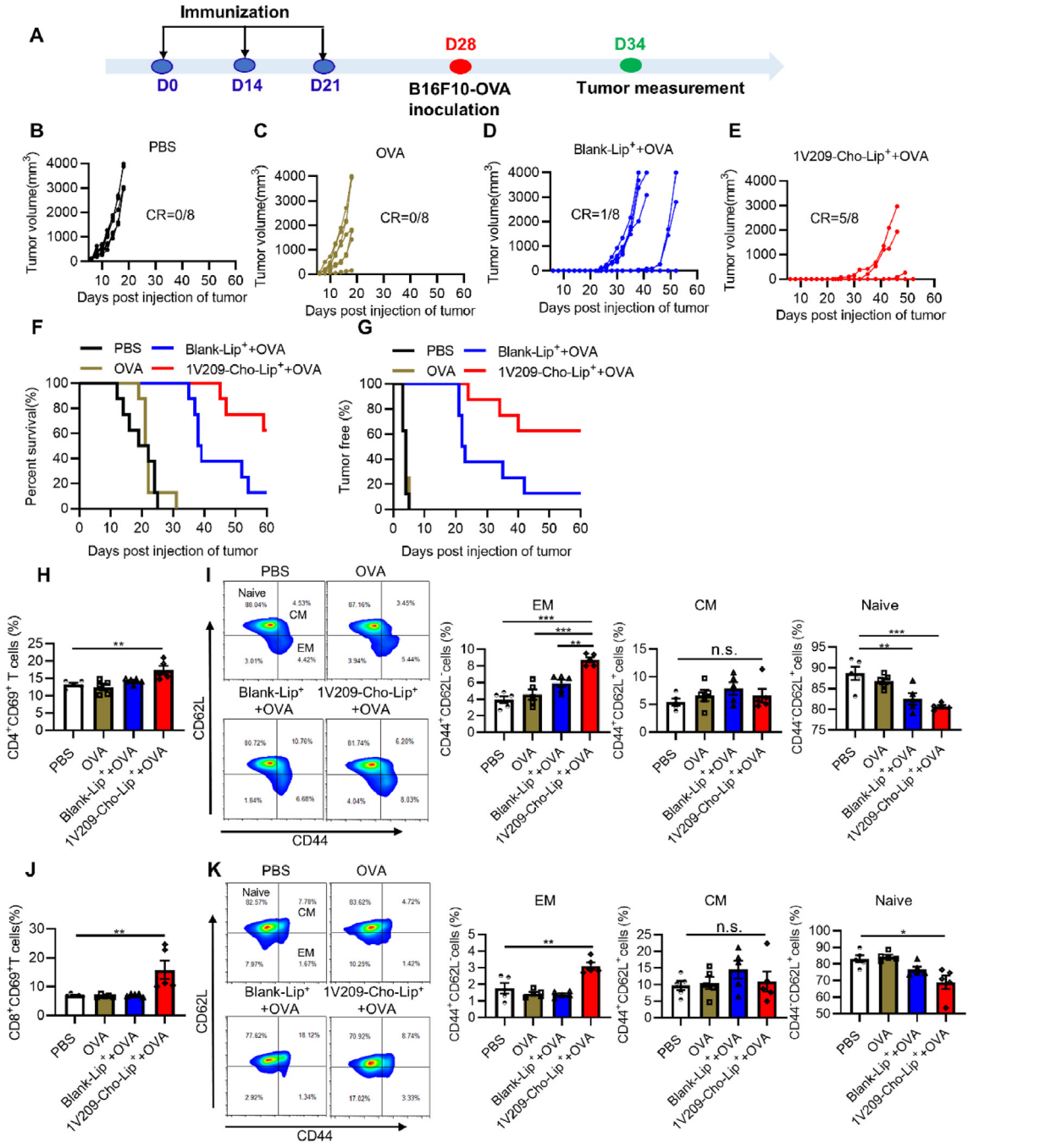

Figure 2 (A) Scheme of immunizations. (B–E) Individual tumor growth curves are shown. CR, complete regression. (F) Percentage survival rate of mice following tumor challenge. (G) Percentage of mice remaining tumor-free after tumor challenge. (H) Quantification of active $CD4^+$ T cells in inguinal LNs. (I) Representative flow cytometry plots and quantification of effector memory $CD4^+$ T cells (EM), central memory $CD4^+$ T cells (CM), and naïve $CD4^+$ T cells (Naive) in inguinal LNs. (J) Quantification of active $CD8^+$ T cells in drain inguinal LNs. (K) Representative flow cytometry plots and quantification of effector memory $CD8^+$ T cells (EM), central memory $CD8^+$ T cells (CM), and naïve $CD8^+$ T cells (Naive) in inguinal LNs. Data are presented as mean ± SEM ($n = 5$). $^*P < 0.05$, $^{**}P < 0.01$, $^{***}P < 0.001$. n.s., not significant.

(Supporting Information Fig. S4). As depicted in Fig. 2I and K, compared to other groups, treatment with 1V209-Cho-Lip^++OVA increased the percentage of effector memory T cells ($CD44^+CD62L^-$) among both $CD4^+$ and $CD8^+$ T cells, while reducing the proportion of naïve T cells ($CD44^-CD62L^+$) among both populations. These results suggest that 1V209-Cho-Lip^++OVA elicits robust memory T cell responses and confers potent protection against tumor recurrence. It has been found that $TCF1^+PD\text{-}1^+CD8^+$ T cells in the LNs with a stem-like phenotype preserve the ongoing anti-tumor immune response, and demonstrate enhanced expansion following ICB therapy[40-42]. After 1V209-Cho-Lip^++OVA immunization, the proportion of stem-

like CD8$^+$ T cells increased within drain inguinal LNs (Fig. 3A and Fig. S3C), suggesting its potential to enhance immune checkpoint blockade therapy.

Then we assessed the splenocytes from thrice immunized mice using FACS, 1V209-Cho-Lip$^+$+OVA immunization significantly increased the frequency of CD4$^+$, activated CD4$^+$ T and CD8$^+$ T

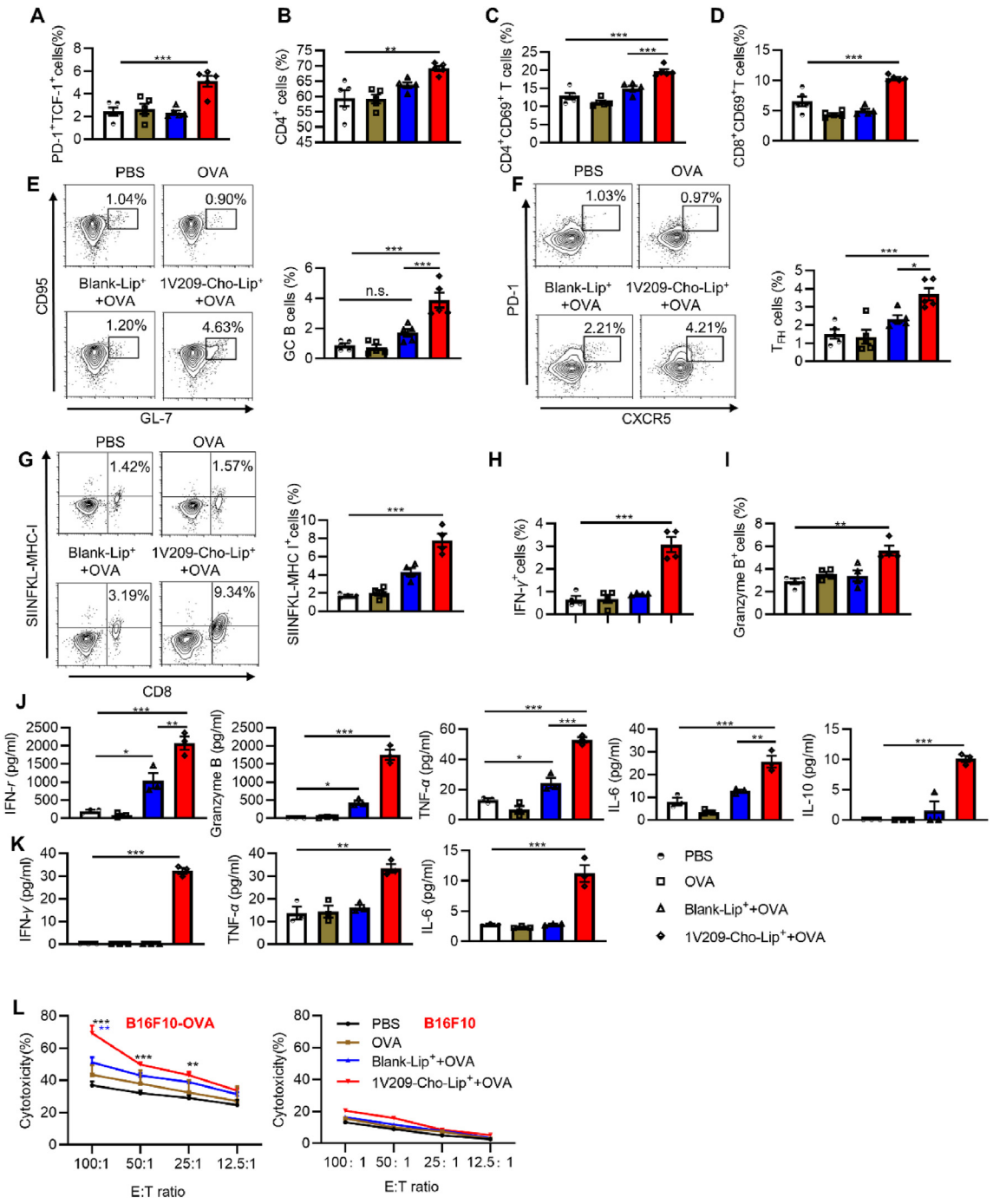

Figure 3 1V209-Cho-Lip$^+$+OVA elicited robust cellular immune responses in mice. (A) Quantification of stem-like CD8$^+$ T cells in inguinal LNs. (B−D) Quantification of (B) CD4$^+$ T cells, (C) activated CD4$^+$ T and (D) CD8$^+$ T cells in spleens. (E) Representative flow cytometry pictures and frequency of GC B cells (GL7$^+$ CD95$^+$ CD19$^+$) in inguinal LNs B cell population. (F) Representative flow cytometry pictures and frequency of T_{FH} cells (CXCR5$^+$ PD-1$^+$ CD4$^+$) in the CD4 T cell population from inguinal LNs. (G) Representative flow cytometry plots and frequency OVA-specific CD8 T cells bearing a T-cell receptor specific for $OVA_{257-264}$-H2Kb tetramer. (H and I) Splenocytes from immunized mice were restimulated $OVA_{257-264}$ *ex vivo*, and the percentages of (H) IFN-γ^+ and (I) Granzyme B$^+$ among CD8α^+ splenocytes are shown. (J) Cytokine production including IFN-γ, Granzyme B, TNF-α, IL-6, and IL-10 after *ex vivo* stimulation of splenocytes for 72 h is presented. (K) Secretion levels of IFN-γ, TNF-α, and IL-6 were measured in the serum samples from immunized mice. (L) The OVA-specific killing ability of CD8$^+$ T cells on tumors. Data are presented as mean ± SEM (n = 3−4). *P < 0.05, **P < 0.01, ***P < 0.001. n.s., not significant.

cells compared with other groups (Fig. 3B−D). To further explore whether 1V209-Cho-Lip$^+$+OVA could significantly enhance GC responses in mice, which is vital to generate the matured plasma cells and the memory B cells that contribute to mediate long term protective immunity[43]. We investigated GC B cell and T_{FH} responses in drain inguinal LNs and spleen of animals immunized with 1V209-Cho-Lip$^+$+OVA. A high frequency of GC B cells was induced in both the drain inguinal LNs and spleen of animals vaccinated with the 1V209-Cho-Lip$^+$+OVA, and this was significantly higher than that induced by Blank-Lip$^+$+OVA (Fig. 3E and Supporting Information Fig. S5A). A corresponding and significant increase in GC T_{FH} was also observed in the draining inguinal LNs and spleen (Fig. 3F and Fig. S5B). These results suggest that vaccination with 1V209-Cho-Lip$^+$+OVA induces an enhanced GC response in draining inguinal LNs and spleen comparison with other groups, thereby promoting the establishment of long-term immunological memory.

Meanwhile, we isolated splenocytes from immunized mice and subsequently incubated them with CD8$^+$-specific $OVA_{257-264}$ peptides *in vitro*. The results demonstrated that vaccination with 1V209-Cho-Lip$^+$+OVA significantly enhanced the abundance of OVA-specific CD8$^+$ T cells compared to PBS (4.6-fold), OVA (3.89-fold), and Blank-Lip$^+$+OVA groups (1.80-fold) as detected by PE-conjugated $OVA_{257-264}$-bound H-2kb tetramer (Fig. 3G). Furthermore, immunization with 1V209-Cho-Lip$^+$+OVA markedly elevated the percentages of CD8$^+$ IFN-γ or granzyme B-producing CTLs (Fig. 3H and I) and enhanced the secretion of IFN-γ and granzyme B (Fig. 3J). 1V209-Cho-Lip$^+$+OVA also dramatically increased the secretion of TNF-α, IL-6 and IL-10 (Fig. 3J). Similar results were also found in the serum of the immunized mice. As shown in Fig. 3K, immunization with 1V209-Cho-Lip$^+$+OVA promoted robust secretion of IFN-γ, TNF-α as well as IL-6 in the serum. The cytotoxic T cell assays were used to evaluate the tumor-specific killing function of CD8$^+$ T cells (Fig. 3L). Briefly, the lymphocytes (effector cells) from the immunized mice with 1V209-Cho-Lip$^+$+OVA, Blank-Lip$^+$+OVA, OVA or PBS were cocultured with antigen ($OVA_{257-264}$), followed by incubation with CFSE-labeled B16F10-OVA tumor cells (target cells) or B16F10 tumor cells (negative control target cells). As shown in Fig. 3L, the 1V209-Cho-Lip$^+$+OVA group exhibited significant cytotoxicity against B16F10-OVA melanoma at increasing ratios of effector to target cells. However, no noticeable difference was observed in the cytotoxic effect against B16F10 melanoma, indicating specific elimination of OVA target cells by 1V209-Cho-Lip$^+$+OVA. The aforementioned results collectively demonstrate the potent ability of the 1V209-Cho-Lip$^+$+OVA nanovaccine to induce robust T-cell immune responses *in vivo*.

3.6. *The long-term immune memory in vivo elicited by 1V209-Cho-Lip$^+$+OVA*

To assess the ability of 1V209-Cho-Lip$^+$+OVA to promote persistent memory immunity and prevent tumor formation, mice were injected with B16F10-OVA tumor cells subcutaneously after 180 days from the initial vaccination (Fig. 4A) and monitored for a period of 20 days. The sizes of tumors at day 20 post-inoculation are depicted in Fig. 4B−E. Notably, immunization with 1V209-Cho-Lip$^+$+OVA resulted in robust and enduring immunological memory against tumor growth, as evidenced by nearly complete rejection of the inoculated B16F10-OVA tumor cells by all vaccinated mice on Day 20 (Fig. 4E and F). Although tumor formation was observed in the mice immunization with Blank-Lip$^+$+OVA until days 16 post-B16F10-OVA inoculation, 60% of the mice failed to prevent tumor formation at 20 days (Fig. 4D and F). Tumor formation was observed 4−8 days after B16F10-OVA inoculation in almost all animals immunized with PBS and OVA (Fig. 4B, C and F). Long-lived memory B cells (BMEM) form a vital part of immunological memory, providing rapid antibody responses to reinfection[44,45]. BMEM in bone marrow and blood were evaluated by flow cytometry (Fig. 4G and Supporting Information Fig. S6A and S6B), mice immunized with 1V209-Cho-Lip$^+$+OVA exhibited a significantly higher frequency of BMEM than that of other groups. Given the crucial role of OVA-specific memory T-cells in eliminating OVA-expressing tumor cells, we conducted an analysis of tumor-specific CD8$^+$ T-cells by the IFN-γ ELISPOT assay. Our data revealed a notable increase in the quantities of IFN-γ^+ CD8$^+$ T cells in spleen and blood following immunization with 1V209-Cho-Lip$^+$+OVA (Fig. 4H and I). In contrast, no substantial elevation in tumor-specific CD8$^+$ memory T-cell numbers was observed in either the spleen or blood for mice belonging to the other three groups (Fig. 4H and I). Furthermore, serum titrations were performed to assess total IgG and IgG2a subtypes at five and six months post-first immunization (Fig. 4A and Fig. S6C and S6D). Notably, administration of 1V209-Cho-Lip$^+$+OVA resulted in significantly higher total IgG and IgG2a titers compared to Blank-Lip$^+$+OVA at both time points (Fig. S6C and S6D). These findings suggest that immunization with 1V209-Cho-Lip$^+$+OVA induces a robust and persistent humoral as well as cellular anti-OVA specific immune response capable of eradicating OVA-expressing tumors.

3.7. *Therapeutic efficacy of the 1V209-Cho-Lip$^+$+OVA combination with anti-PD-1 checkpoint blockade*

Subsequently, we conducted further investigations into the therapeutic immunization in established B16F10-OVA tumors mice using 1V209-Cho-Lip$^+$+OVA to explore its antitumor effect. Notably, our findings revealed an augmented proportion of stem-like CD8$^+$ T cells within the inguinal LNs following 1V209-Cho-Lip$^+$+OVA immunization (Fig. 3A), which could potentially enhance the efficacy of ICB[40-42]. Consequently, we further explored the synergistic antitumor effects by combining 1V209-Cho-Lip$^+$+OVA immunization with anti-PD-1 treatment. The schematic of the drug treatment as shown in Fig. 4J. Mice that received PBS alone exhibited a median survival time of only 20 days, and all mice succumbed to tumor inoculation by day 26 (Fig. 4K and Q). The OVA group and anti-PD-1 group exhibited similar efficacy to the PBS group, with an average survival of 23 and 24 days, respectively (Fig. 4L, O and Q). While Blank-Lip$^+$+OVA only showed a mild tumor inhibition effect, with an average survival of 31 days, all mice succumbed to the tumor within 41 days after inoculation (Fig. 4M and Q). 1V209-Cho-Lip$^+$+OVA significantly prohibited tumor progression, surviving an average of 43 d (Fig. 4N and Q). Notably, combination immunotherapy using 1V209-Cho-Lip$^+$+OVA in conjunction with anti-PD-1 further suppressed tumor progression, resulting in a remarkable survival rate of 75% after the designated monitoring duration (60 days) (Fig. 4P and Q). The therapeutic efficacy of 1V209-Cho-Lip$^+$+OVA surpassed that of other groups in terms of inhibiting tumor growth and improving both survival time and rate. Furthermore, immunization with 1V209-Cho-Lip$^+$+OVA exhibited a potential to augment ICB therapy.

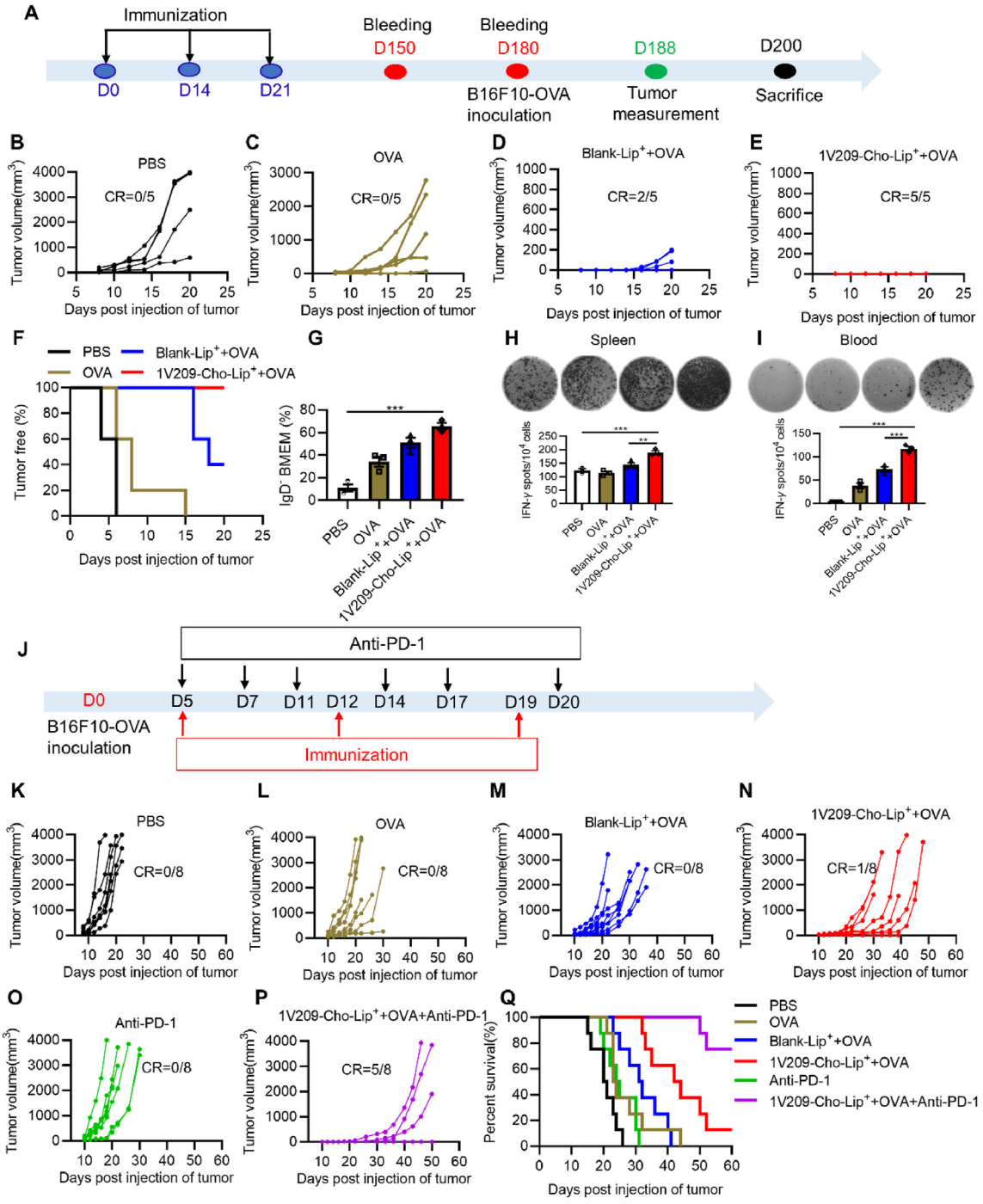

Figure 4 (A) Scheme of the immunization procedures and experimental design. (B−E) Curves depicting the growth of tumors in individual mice that were injected with B16F10-OVA tumor cells. CR, complete regression. (F) Percentage of mice remaining tumor-free after tumor challenge. (G) Quantification of BMEM in bone marrow. (H and I) ELISPOT was used to determine the abundance of IFN-γ^+ splenocytes (H) and cells in the blood (I). Representative images of ELISPOT wells are shown. (J) Schematic representation depicting therapeutic immunization against established B16F10-OVA tumors. (K−P) Curves depicting the growth of tumors in individual mice. CR, complete regression. (Q) Percentage survival rate of mice following tumor challenge. Data are presented as mean ± SEM ($n = 3$). *$P < 0.05$, **$P < 0.01$, ***$P < 0.001$.

3.8. Prophylactic and therapeutic efficacy of 1V209-Cho-Lip$^+$+OVA in E.G7-OVA tumor model

To further evaluate the antitumor efficacy of the 1V209-Cho-Lip$^+$+OVA nanovaccine in both cancer prevention and therapeutic contexts, we generated another OVA-expressing mouse T lymphoma cell line E.G7-OVA for the tumor experiment (Fig. 5A and G). C57BL/6J mice were assigned into four different groups: a PBS group, an OVA group, a Blank-Lip$^+$+OVA group, and a 1V209-Cho-Lip$^+$+OVA group. All

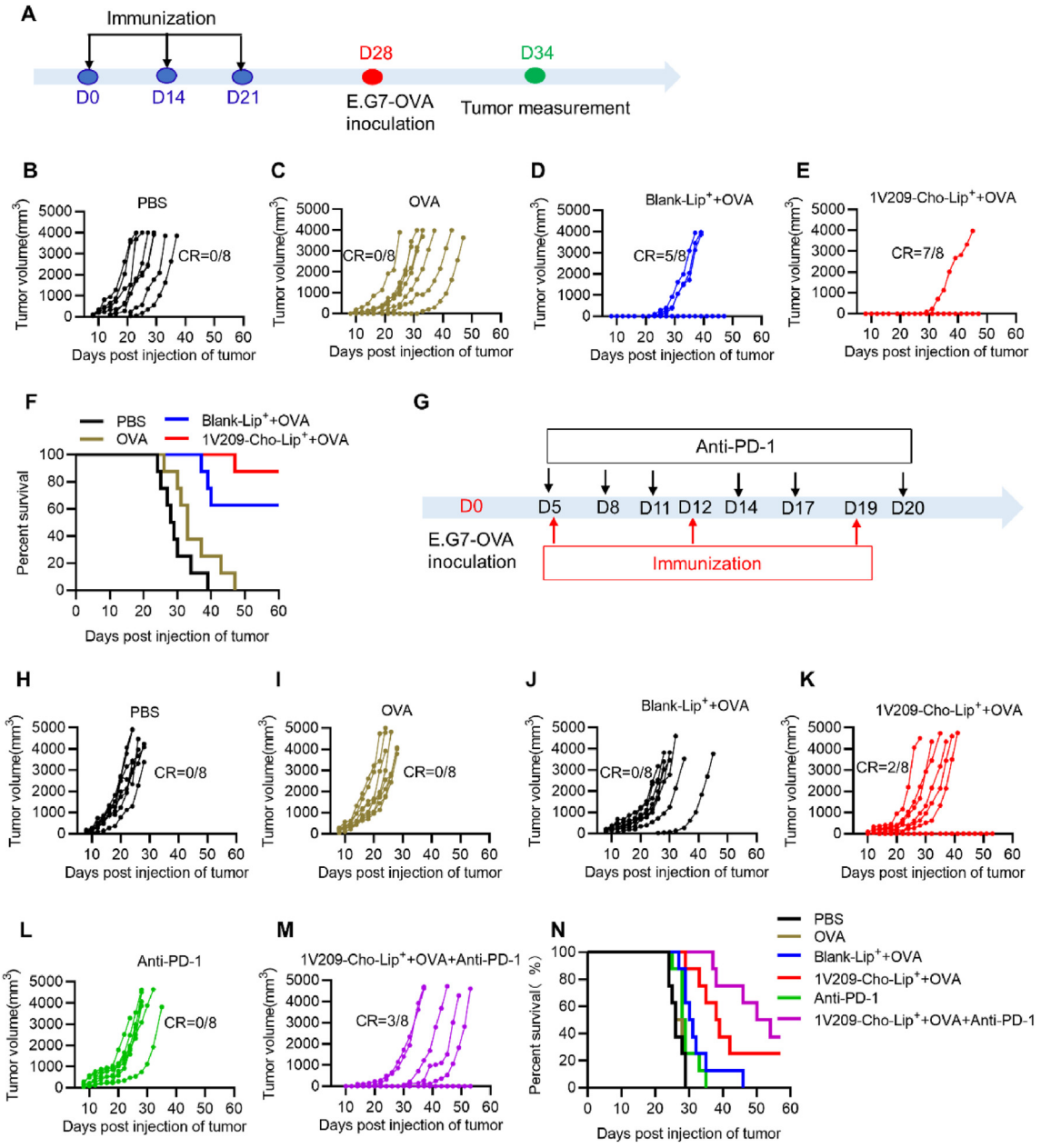

Figure 5 *In vivo* prophylactic and therapeutic efficacy of the 1V209-Cho-Lip^{+}+OVA vaccine in E.G7-OVA syngeneic allograft tumor mode. (A) Experimental design for tumor challenge in the immune-prophylaxis group was illustrated. (B−E) Curves depicting the growth of tumors in individual mice. CR, complete regression. (F) Percentage survival rate of mice following tumor challenge. (G) Schematic of therapeutic immunization against established E.G7-OVA tumors. (H−M) Curves depicting the growth of tumors in individual mice. CR, complete regression. (N) Percentage survival rate of mice following tumor challenge.

vaccines were intramuscularly injected on Days 0, 14, 21 (Fig. 5A). After a week following the last vaccination, E.G7-OVA T lymphoma cells were inoculated. The 1V209-Cho-Lip^{+}+OVA nanovaccine group exhibited superior tumor inhibition and significantly prolonged survival time compared to the Blank-Lip^{+}+OVA group, OVA group, and PBS group (Fig. 5B−F). Furthermore, when employed as a therapeutic vaccine after tumor inoculation (Fig. 5G), the 1V209-Cho-Lip^{+}+OVA nanovaccine effectively suppressed E.G7-OVA tumor growth and extended mouse survival (Fig. 5H−K and N). Notably, the combination of 1V209-Cho-Lip^{+}+OVA with anti-PD-1 resulted in further enhancement of therapeutic efficacy (Fig. 5L and M) and prolonged survival time (Fig. 5N). These results indicate that 1V209-Cho-Lip^{+}+OVA exhibits robust antitumor effects in both E.G7-OVA prophylactic and therapeutic models.

3.9. *Safety evaluation*

The safety of the 1V209-Cho-Lip^{+}+OVA vaccine was evaluated by conducting a comprehensive analysis of complete blood count (Fig. 6A) and serum chemistry panel (Fig. 6B). No statistically significant differences were found among all groups. Additionally, no histological alterations were detected in the heart, liver, spleen, lungs, and kidney of the vaccinated mice (Fig. 6C).

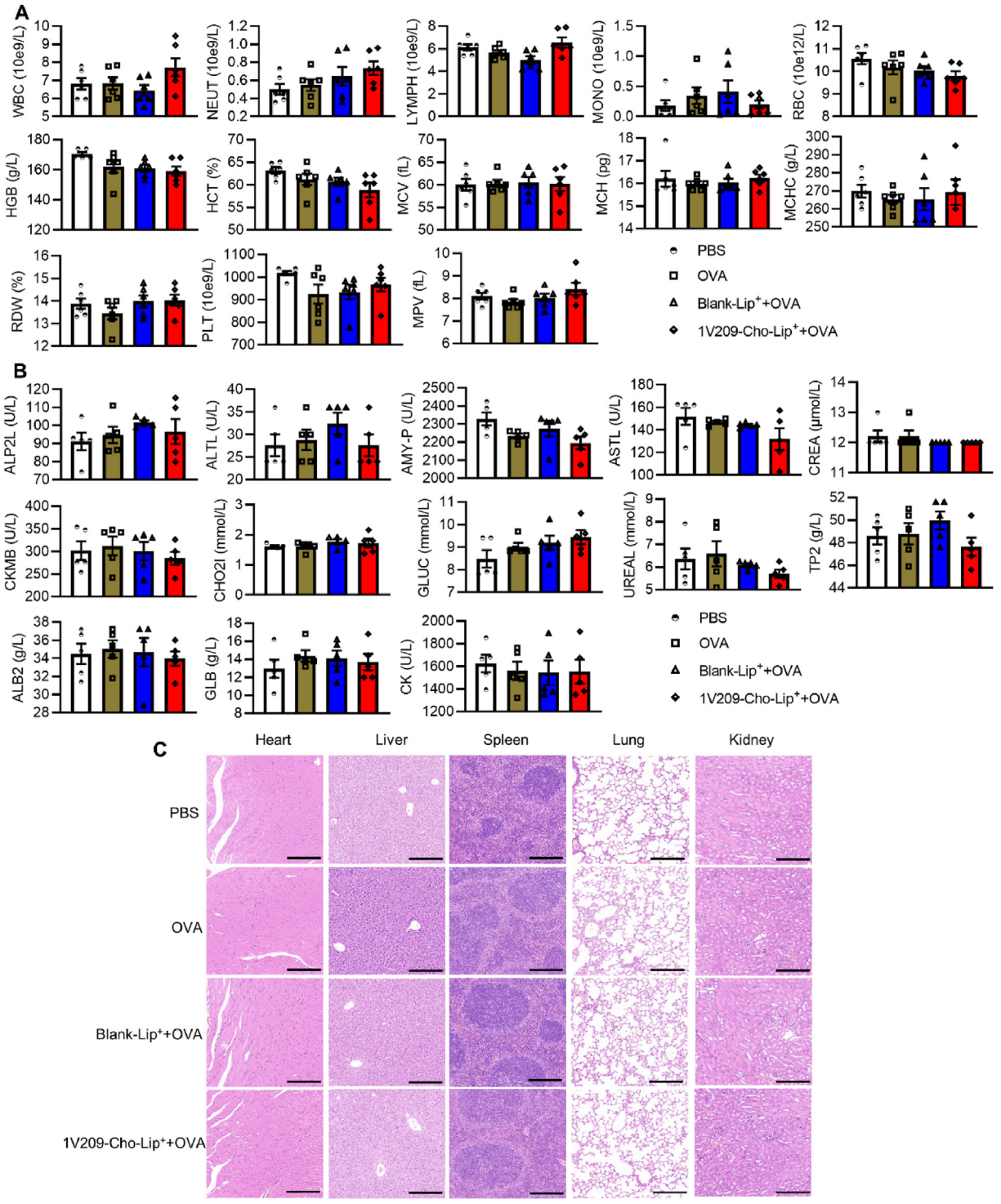

Figure 6 Tolerability of 1V209-Cho-Lip^{+}+OVA was evaluated in C57BL/6J mice through intramuscular immunization with 1V209-Cho-Lip^{+}+OVA on Days 0, 14, and 21. On Day 28, blood samples were collected to assess complete blood count parameters (A) and biochemical indexes (B). (C) Vital organs were subjected to hematoxylin and eosin staining for histopathological examination. Scale bar = 200 μm. Data are presented as mean ± SEM (n = 5).

4. Conclusions

Currently, adjuvants remain the most crucial strategy for enhancing the efficacy of conventional and next-generation vaccines. In this study, we have developed a cholesterolized TLR7 agonist cationic liposomes vaccine platform (1V209-Cho-Lip^{+}+OVA) that not only induces *in vitro* maturation of DCs but also significantly enhances cross-presentation of extracellular antigens by DCs. The 1V209-Cho-Lip^{+}+OVA vaccine platform efficiently co-delivers the model antigen (OVA) and

cholesterolized TLR7 agonist (1V209-Cho) to lymph nodes for presentation to DCs. Our findings demonstrate that 1V209-Cho-Lip$^+$+OVA could induce extremely potent and durable T cell responses, long-lasting T cell immunological memory, as well protective immunity. Upon prophylactic vaccination, 1V209-Cho-Lip$^+$+OVA demonstrates superior efficacy in delaying tumor development and increasing survival rates. Moreover, therapeutic tumor challenge experiments reveal that 1V209-Cho-Lip$^+$+OVA inhibits tumor progression significantly. More strikingly, the combination of 1V209-Cho-Lip$^+$+OVA with anti-PD-1 effectively suppresses tumor immunosuppression and achieves potent therapeutic antitumor effects. In conclusion, the present cholesterolized TLR7 agonist cationic liposomal vaccine candidate represents a promising approach for co-encapsulation of antigens and adjuvants, offering great potential as a highly potent and durable preventive vaccine against cancer in humans.

Acknowledgments

This work was supported by the National Science Foundation for Excellent Young Scholars (32122052, China) and National Natural Science Foundation Regional Innovation and Development (No. U19A2003, China).

Author contributions

Xiawei Wei and Qiang Pu designed the research. Dandan Wan carried out the experiments and performed data analysis. Ziyi Bai, Yu Zhang, Li Chen, Haiying Que, Tianxia Lan, Weiqi Hong, Jiayu Huang and Cai He participated part of the experiments. Yuquan Wei provided experimental drugs and quality control. Dandan Wan wrote the manuscript. Xiawei Wei revised the manuscript. All of the authors have read and approved the final manuscript.

Conflicts of interest

The authors have no conflicts of interest to declare.

Appendix A. Supporting information

Supporting information to this article can be found online at https://doi.org/10.1016/j.apsb.2024.06.006.

References

1. Li X, Cai XY, Zhang ZZ, Ding YX, Ma RJ, Huang F, et al. Mimetic heat shock protein mediated immune process to enhance cancer immunotherapy. *Nano Lett* 2020;**20**:4454−63.
2. Jiang X, Yi L, Li C, Wang HX, Xiong W, Li Y, et al. Mitochondrial disruption nanosystem simultaneously depressed programmed death ligand-1 and transforming growth factor-β to overcome photodynamic immunotherapy resistance. *ACS Nano* 2024;**18**:3331−48.
3. Yi L, Jiang X, Zhou ZG, Xiong W, Xue F, Liu Y, et al. A Hybrid nanoadjuvant simultaneously depresses PD-L1/TGF-β1 and activates cGAS-STING pathway to overcome radio-immunotherapy resistance. *Adv Mater* 2024;**36**:e2304328.
4. Yang DY, Luo X, Lian QH, Gao LQ, Wang CX, Qi XX, et al. Fully synthetic Tn-based three-component cancer vaccine using covalently linked TLR4 ligand MPLA and iNKT cell agonist KRN-7000 as built-in adjuvant effectively protects mice from tumor development. *Acta Pharm Sin B* 2022;**12**:4432−45.
5. Wilson JT, Keller S, Manganiello MJ, Cheng C, Lee CC, Opara C, et al. pH-Responsive nanoparticle vaccines for dual-delivery of antigens and immunostimulatory oligonucleotides. *ACS Nano* 2013;**7**:3912−25.
6. Fang RH, Hu CM, Luk BT, Gao W, Copp JA, Tai Y, et al. Cancer cell membrane-coated nanoparticles for anticancer vaccination and drug delivery. *Nano Lett* 2014;**14**:2181−8.
7. Shao K, Singha S, Clemente-Casares X, Tsai S, Yang Y, Santamaria P. Nanoparticle-based immunotherapy for cancer. *ACS Nano* 2015;**9**:16−30.
8. Marrack P, Mckee AS, Munks MW. Towards an understanding of the adjuvant action of aluminium. *Nat Rev Immunol* 2009;**9**:287−93.
9. Banchereau J, Briere F, Caux C, Davoust J, Lebecque S, Liu YJ, et al. Immunobiology of dendritic cells. *Annu Rev Immunol* 2000;**18**:767−811.
10. Liu Q, Chen XM, Jia J, Zhang WF, Yang TY, Wang LY, et al. pH-Responsive poly(D,L-lactic-*co*-glycolic acid) nanoparticles with rapid antigen release behavior promote immune response. *ACS Nano* 2015;**9**:4925−38.
11. Trombetta ES, Mellman I. Cell biology of antigen processing *in vitro* and *in vivo*. *Annu Rev Immunol* 2005;**23**:975−1028.
12. Hou B, Reizis B, Defranco AL. Toll-like receptors activate innate and adaptive immunity by using dendritic cell-intrinsic and -extrinsic mechanisms. *Immunity* 2008;**29**:272−82.
13. Macleod H, Wetzler LM. T cell activation by TLRs: a role for TLRs in the adaptive immune response. *Sci STKE* 2007;**2007**:pe48.
14. Wang C, Liu P, Zhuang Y, Li P, Jiang BL, Pan H, et al. Lymphatic-targeted cationic liposomes: a robust vaccine adjuvant for promoting long-term immunological memory. *Vaccine* 2014;**32**:5475−83.
15. Zhang WF, Wang LY, Liu Y, Chen XM, Liu Q, Jia JL, et al. Immune responses to vaccines involving a combined antigen-nanoparticle mixture and nanoparticle-encapsulated antigen formulation. *Biomaterials* 2014;**35**:6086−97.
16. Wei C, Dong X, Liang J, Zhang Y, Zhu DW, Kong DL, et al. Real-time imaging tracking of a dual fluorescent vaccine delivery system based on ovalbumin loaded zinc phthalocyanine-incorporated copolymer nanoparticles. *J Biomed Nanotechnol* 2019;**15**:100−12.
17. Zhu GZ, Zhang FW, Ni QQ, Niu G, Chen XY. Efficient nanovaccine delivery in cancer immunotherapy. *ACS Nano* 2017;**11**:2387−92.
18. Reed SG, Orr MT, Fox CB. Key roles of adjuvants in modern vaccines. *Nat Med* 2013;**19**:1597−608.
19. Shah RR, Hassett KJ, Brito LA. Overview of vaccine adjuvants: introduction, history, and current status. *Methods Mol Biol* 2017;**1494**:1−13.
20. Beutler BA. TLRs and innate immunity. *Blood* 2009;**113**:1399−407.
21. Kawai T, Akira S. The role of pattern-recognition receptors in innate immunity: update on Toll-like receptors. *Nat Immunol* 2010;**11**:373−84.
22. Kawasaki T, Kawai T. Toll-like receptor signaling pathways. *Front Immunol* 2014;**5**:461.
23. Black M, Trent A, Tirrell M, Olive C. Advances in the design and delivery of peptide subunit vaccines with a focus on toll-like receptor agonists. *Expert Rev Vaccin* 2010;**9**:157−73.
24. Fan YC, Kuai R, Xu Y, Ochyl LJ, Irvine DJ, Moon JJ. Immunogenic cell death amplified by co-localized adjuvant delivery for cancer immunotherapy. *Nano Lett* 2017;**17**:7387−93.
25. Jin JW, Tang SQ, Rong MZ, Zhang MQ. Synergistic effect of dual targeting vaccine adjuvant with aminated β-glucan and CpG-oligodeoxynucleotides for both humoral and cellular immune responses. *Acta Biomater* 2018;**78**:211−23.
26. Xia QM, Gong CN, Gu FF, Wang Z, Hu CL, Zhang LJ, et al. Functionalized multi-walled carbon nanotubes for targeting delivery of immunostimulatory CpG oligonucleotides against prostate cancer. *J Biomed Nanotechnol* 2018;**14**:1613−26.
27. Baenziger S, Heikenwalder M, Johansen P, Schlaepfer E, Hofer U, Miller RC, et al. Triggering TLR7 in mice induces immune activation and lymphoid system disruption, resembling HIV-mediated pathology. *Blood* 2009;**113**:377−88.

28. Dovedi SJ, Melis MH, Wilkinson RW, Adlard AL, Stratford IJ, Honeychurch J, et al. Systemic delivery of a TLR7 agonist in combination with radiation primes durable antitumor immune responses in mouse models of lymphoma. *Blood* 2013;**121**:251−9.
29. Dowling JK, Mansell A. Toll-like receptors: the swiss army knife of immunity and vaccine development. *Clin Transl Immunol* 2016;**5**:e85.
30. Wan DD, Que HY, Chen L, Lan TX, Hong WQ, He C, et al. Lymph-node-targeted cholesterolized TLR7 agonist liposomes provoke a safe and durable antitumor response. *Nano Lett* 2021;**21**:7960−9.
31. Hubbell JA, Thomas SN, Swartz MA. Materials engineering for immunomodulation. *Nature* 2009;**462**:449−60.
32. Ma YF, Zhuang Y, Xie XF, Wang C, Wang F, Zhou DM, et al. The role of surface charge density in cationic liposome-promoted dendritic cell maturation and vaccine-induced immune responses. *Nanoscale* 2011;**3**:2307−14.
33. Zheng CJ, Luo WJ, Liu Y, Chen JS, Deng H, Zhou ZG, et al. Killing three birds with one stone: multi-stage metabolic regulation mediated by clinically useable berberine liposome to overcome photodynamic immunotherapy resistance. *Chem Eng J* 2022;**454**:140164.
34. Wang SJ, Zhou ZG, Hu R, Dong MY, Zhou XB, Ren SY, et al. Metabolic intervention liposome boosted lung cancer radioimmunotherapy *via* hypoxia amelioration and PD-L1 restraint. *Adv Sci (Weinh)* 2023;**10**:e2207608.
35. Chen W, Yan W, Huang L. A simple but effective cancer vaccine consisting of an antigen and a cationic lipid. *Cancer Immunol Immunother* 2008;**57**:517−30.
36. Vangasseri DP, Cui Z, Chen W, Hokey DA, Falo Jr LD, Huang L. Immunostimulation of dendritic cells by cationic liposomes. *Mol Membr Biol* 2006;**23**:385−95.
37. Heath WR, Carbone FR. Cross-presentation, dendritic cells, tolerance and immunity. *Annu Rev Immunol* 2001;**19**:47−64.
38. Henriksen-Lacey M, Bramwell VW, Christensen D, Agger EM, Andersen P, Perrie Y. Liposomes based on dimethyldioctadecylammonium promote a depot effect and enhance immunogenicity of soluble antigen. *J Control Release* 2010;**142**:180−6.
39. Henriksen-Lacey M, Christensen D, Bramwell VW, Lindenstrøm T, Agger EM, Andersen P, et al. Comparison of the depot effect and immunogenicity of liposomes based on dimethyldioctadecylammonium (DDA), 3β-[*N*-(*N*′,*N*′-dimethylaminoethane)carbomyl] cholesterol (DC-Chol), and 1,2-dioleoyl-3-trimethylammonium propane (DOTAP): prolonged liposome retention mediates stronger Th1 responses. *Mol Pharm* 2011;**8**:153−61.
40. Connolly KA, Kuchroo M, Venkat A, Khatun A, Wang J, William I, et al. A reservoir of stem-like $CD8^+$ T cells in the tumor-draining lymph node preserves the ongoing antitumor immune response. *Sci Immunol* 2021;**6**:eabg7836.
41. Im SJ, Hashimoto M, Gerner MY, Lee J, Kissick HT, Burger MC, et al. Defining $CD8^+$ T cells that provide the proliferative burst after PD-1 therapy. *Nature* 2016;**537**:417−21.
42. Siddiqui I, Schaeuble K, Chennupati V, Fuertes Marraco SA, Calderon-Copete S, Pais Ferreira D, et al. Intratumoral $Tcf1^+PD\text{-}1^+CD8^+$T cells with stem-like properties promote tumor control in response to vaccination and checkpoint blockade immunotherapy. *Immunity* 2019;**50**:195−211.e10.
43. Kasturi SP, Rasheed MaU, Havenar-Daughton C, Pham M, Legere T, Sher ZJ, et al. 3M-052, a synthetic TLR-7/8 agonist, induces durable HIV-1 envelope-specific plasma cells and humoral immunity in nonhuman primates. *Sci Immunol* 2020;**5**:eabb1025.
44. Hartley GE, Edwards ESJ, Aui PM, Varese N, Stojanovic S, Mcmahon J, et al. Rapid generation of durable B cell memory to SARS-CoV-2 spike and nucleocapsid proteins in COVID-19 and convalescence. *Sci Immunol* 2020;**5**:eabf8891.
45. Müller-Winkler J, Mitter R, Rappe JCF, Vanes L, Schweighoffer E, Mohammadi H, et al. Critical requirement for BCR, BAFF, and BAFFR in memory B cell survival. *J Exp Med* 2021;**218**:e20191393.